

# A Distributed Bragg Reflector Silicon Evanescent Laser

Alexander W. Fang, *Student Member, IEEE*, Brian R. Koch, *Student Member, IEEE*, Richard Jones, *Member, IEEE*, Erica Lively, Di Liang, *Member, IEEE*, Ying-Hao Kuo, and John E. Bowers, *Fellow, IEEE*

**Abstract**—We report a distributed Bragg reflector silicon evanescent laser operating continuous wave at 1596 nm. The lasing threshold and maximum output power are 65 mA and 11 mW, respectively. The device generates open eye-diagrams under direct modulation at data rates up to 4 Gb/s.

**Index Terms**—Hybrid integration, semiconductor lasers, silicon-on-insulator technology.

## I. INTRODUCTION

**H**YBRID integration is currently being investigated as a method of creating electrically pumped laser sources for silicon photonic integration. This new interest is due to promising developments in the transfer of thin crystalline III–V films to silicon through benzocyclobutene (BCB)-based wafer bonding, direct wafer bonding, and low temperature oxygen plasma-assisted wafer bonding [1]–[3]. These approaches have led to the demonstration of electrically pumped micro-disk and Fabry–Pérot (FP) III–V membrane lasers coupled to silicon waveguides [3], [4] and FP and racetrack hybrid silicon evanescent lasers [5]. These devices allow for the use of electrically pumped III–V gain regions while enabling scalable manufacturing through alignment-free bonding that is absent in conventional gold bump bond die attachment of III–V active devices. Hybrid silicon evanescent lasers (SELs) utilize both III–V regions and silicon waveguide regions within the device, allowing for processing in the silicon region to define the cavity along with lasing properties.

Earlier this year, we demonstrated a distributed feedback (DFB) SEL [6]. A surface corrugated grating was formed at the bonded interface of the silicon waveguide and III–V active region bisecting the optical mode, leading to a high grating strength,  $\kappa$ , of  $240 \text{ cm}^{-1}$ . While high grating strength lasers are advantageous for short and low threshold DFBs, their maximum output power is limited due to their small mode volume. In addition, their short device length also leads to higher thermal impedance. On the other hand, distributed Bragg reflector

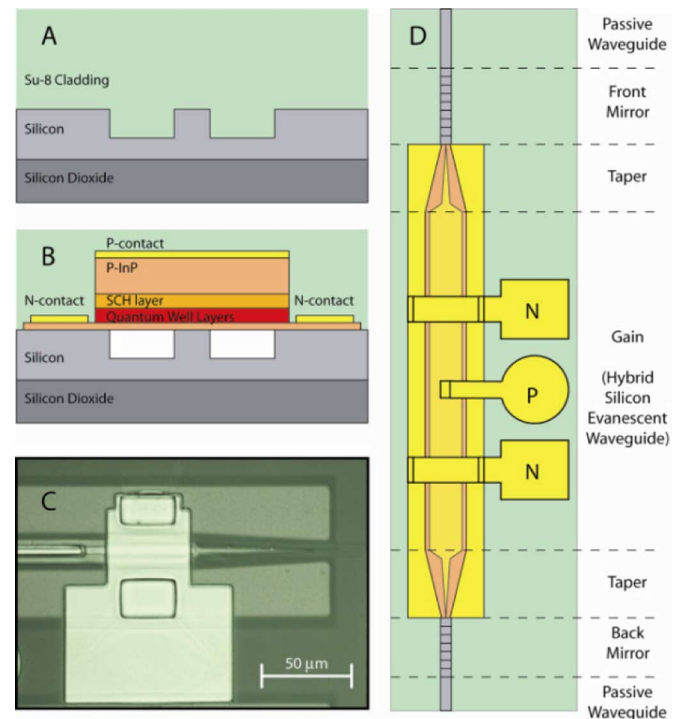


Fig. 1. (a) Passive silicon rib and (b) hybrid silicon evanescent waveguide cross section. (c) Microscope image of a hybrid to passive taper. (d) DBR-SEL top-view topographical structure.

(DBR) lasers occupy a different design space where longer cavities can be employed to reduce the device thermal impedance and increase output powers. We demonstrate here a DBR-SEL where passive silicon gratings are placed on both sides of the active region in order to form a wavelength selective cavity. The  $600\text{-}\mu\text{m}$ -long asymmetric cavity allows for 96% of its 11.5-mW output power to exit one side of the device. We also present test results of direct digital modulation at 2.5 and 4 Gb/s.

## II. DEVICE STRUCTURE

The DBR-SEL is fabricated on the hybrid silicon evanescent waveguide platform as described in [5]. Fig. 1(a) and (b) shows the waveguide cross section of the passive silicon waveguide and the hybrid silicon evanescent waveguide regions, respectively. The silicon waveguide has a width, height, and rib etch depth of 2, 0.7, and  $0.5 \mu\text{m}$ , respectively. This results in silicon and quantum well confinement factors of 66% and 4.4% in the hybrid region.

The device topography [Fig. 1(d)] consists of two passive Bragg reflector mirrors placed  $600 \mu\text{m}$  apart to form an optical cavity. The back and front mirror lengths are  $300 \mu\text{m}$  and  $100 \mu\text{m}$ .

Manuscript received June 23, 2008; revised July 14, 2008. First published August 19, 2008; current version published September 26, 2008. This work was supported in part by a grant from Intel Corporation, in part by the Defense Advanced Research Projects Agency under Program DARPA/MTO DODN, and in part by ARL under Awards W911NF-05-1-0175 and W911NF-04-9-0001.

A. W. Fang, E. Lively, D. Liang, Y.-H. Kuo, and J. E. Bowers are with the Department of Electrical and Computer Engineering, University of California, Santa Barbara, CA 93106 USA (e-mail: awfang@ece.ucsb.edu).

B. R. Koch and R. Jones are with the Photonics Technology Laboratory, Intel Corporation, Santa Clara, CA 95054 USA.

Color versions of some of the figures in this letter are available online at <http://ieeexplore.ieee.org>.

Digital Object Identifier 10.1109/LPT.2008.2003382

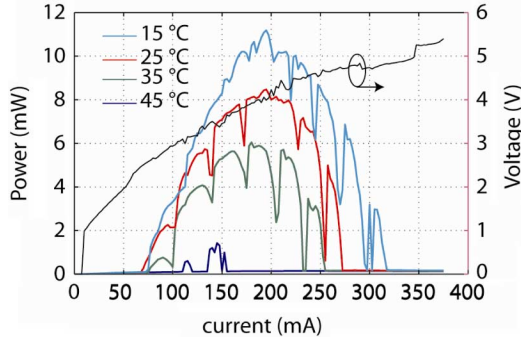


Fig. 2. DBR-SEL  $L$ - $I$ - $V$  curve for various temperatures measured out of the front mirror.

The surface corrugated gratings are formed during silicon processing prior to wafer bonding through e-beam lithography. SU-8 is used to clad the gratings since they have a low index of 2.11 while providing a low capacitance dielectric barrier for the device contacts. The gratings have an etch depth and duty cycle of 25 nm and 75%, respectively, leading to a grating strength,  $\kappa$ , of  $80 \text{ cm}^{-1}$ . The grating  $\kappa$  was measured on grating test structures by measuring the transmission spectra stop band extinction ratio for grating lengths  $L$ , of 50, 100, and  $300 \mu\text{m}$ . The power reflectivity  $R$  of the gratings can be calculated using the following expression [7]:

$$R = \tanh^2(\kappa L)$$

resulting in power reflectivities of 97% and 44% for the back and front mirrors, respectively.

A  $440\text{-}\mu\text{m}$ -long silicon evanescent gain region and two  $80\text{-}\mu\text{m}$ -long tapers [Fig. 1(c)] are placed inside the cavity. The tapers provide an adiabatic transition between the passive silicon regions and the silicon evanescent waveguide regions by varying the width of the upper III-V layers along the length of the taper, reducing the reflection, and allowing for low loss coupling ( $\sim 1.2 \text{ dB}$ ) between these two regions [5]. The tapers are electrically driven in parallel with the gain region in order to minimize absorption.

### III. EXPERIMENTAL RESULTS

The continuous wave laser output power is measured with an integrating sphere at the front mirror of the laser. The front mirror output power-current-voltage ( $L$ - $I$ - $V$ ) characteristic is shown in Fig. 2. The device has a lasing threshold of 65 mA, a maximum front mirror output power of 11 mW, leading to a differential efficiency of 15%. The taper transmission loss can have a significant impact on the threshold current and therefore it affects many important laser characteristics such as wall plug efficiency and resonance frequency. If we use our estimations of the material and laser properties, calculations show that the taper loss of 1.2 dB increases the threshold current by a factor of 2 due to the accumulated loss through four taper transitions in one round trip through the cavity. We estimate that a reduction in the single pass taper losses to 0.5 dB would reduce this factor to 1.2. The laser operates up to a stage temperature of  $45 \text{ }^\circ\text{C}$ . The kinks in the LI are from mode hopping and will be discussed later. The device has a lasing turn-on voltage of 2.6 V and a series resistance of  $11.5 \Omega$ . The lasing spectrum is shown in

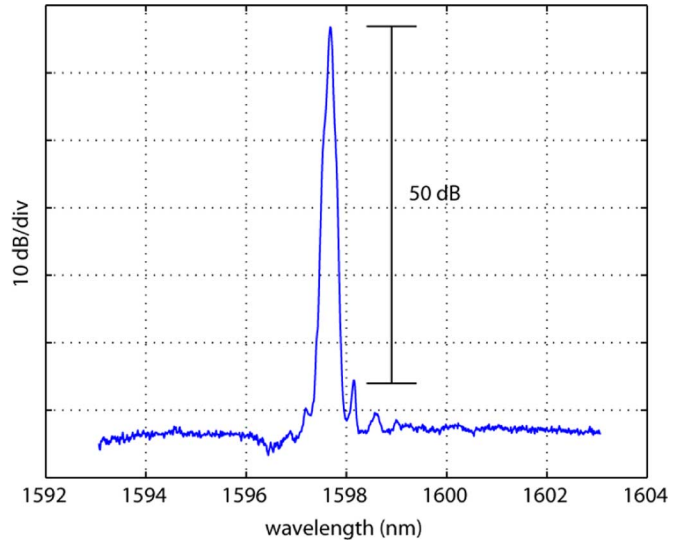


Fig. 3. Optical spectrum of the DBR-SEL driven at 200 mA.

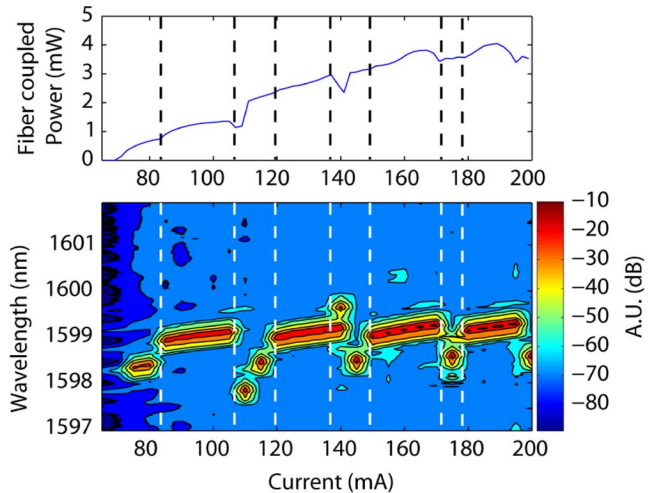


Fig. 4. Fiber coupled  $L$ - $I$  curve and spectrum versus current at a stage temperature of  $18 \text{ }^\circ\text{C}$ .

Fig. 3 with a lasing peak at 1597.5 nm when driven at 200 mA. The device has a free spectral range (FSR) of 0.47 nm, which corresponds to a group index of 3.86 based on the sum of the physical cavity length and mirror penetration depths of 61 and  $42 \mu\text{m}$ . The sidemode suppression ratio is 50 dB.

Fig. 4 shows the lasing spectrum as a function of drive current along with the corresponding  $L$ - $I$  curve. Note that the output power in this case is fiber coupled, which is  $\sim 5 \text{ dB}$  lower than the total output power measured earlier in Fig. 2. It can be seen that as the device heats with larger current injection, the lasing mode moves to longer wavelengths due to the thermo-optic effect in the cavity. When the mode moves far enough from the reflection peak, a longitudinal mode hop to another mode occurs. The mode hopping appears to be chaotic between stable mode positions and the reason for the exact hopping pattern we observed is unknown at this time.

We measured the modulation characteristics of the device by using a bias-T to drive the laser simultaneously with a dc bias current and an radio frequency (RF) signal while measuring the electrooptic (EO) response on a photodetector. Fig. 5 shows the

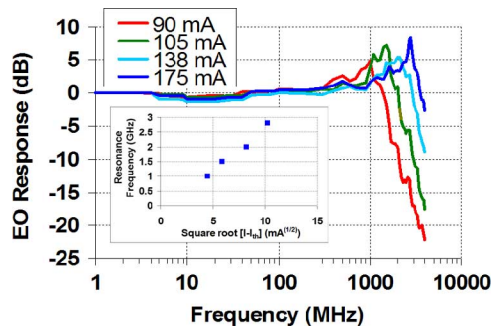


Fig. 5. Photodetected frequency response of the DFB-SEL for three different bias currents with a stage temperature of 18 °C and (inset) plot of resonance frequency versus the square root of current above threshold.

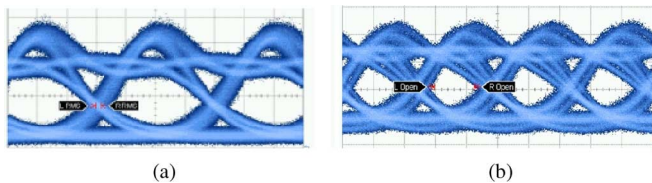


Fig. 6. Eye diagrams of a directly modulated DBR-SEL at (a) 2.5 Gb/s and (b) 4 Gb/s.

photodetected EO response of the laser combined with all connected components under small signal modulation ( $-10$  dBm). S11 measurements indicate that the electrical contact geometry is not limiting the performance of the device, so reflected power has not been factored out of these curves. A 2-pF device capacitance was extracted from the S11 measurement, resulting in an RC limited bandwidth of 7 GHz. Fig. 5 (inset) shows the resonance frequency versus the square root of dc drive current above threshold, which has a roughly linear dependence as expected. Under higher modulation powers the resonance peak becomes significantly dampened. The 3-dB electrical bandwidth at 105 mA is  $\sim 2.5$  GHz.

We directly modulated the laser biased at 105-mA dc current with a 2.5 Gb/s,  $2^{31}-1$  PRBS electrical signal with 20 mW of RF power. The resulting eye diagram is shown in Fig. 6(a). The extinction ratio is 8.7 dB and the fiber coupled output power is  $\sim 0.7$  mW when cooled to 18 °C. Although the output power and modulation bandwidth increases at higher dc currents, the peak-to-peak (P-P) current swing corresponds to a lower P-P output power swing at higher current biases (Fig. 2). This leads to lower extinction ratios at higher current biases unless larger RF modulation powers are used. For example, Fig. 6(b) shows an eye diagram at 4 Gb/s that can be obtained with a dc bias of 135 mA and an RF power of 39 mW. However, in this case the extinction ratio (ER) is closer to 5.5 dB. Improving the laser design to decrease the threshold current and increase the differential gain is expected to significantly improve the modulation bandwidth in future devices.

Fig. 7 shows characteristics of the eye diagrams under different operating conditions. Depending on network requirements, different operating points could be chosen to minimize power dissipation. The differences between uncooled operation and operation at 18 °C result from differences in the output power for a given dc bias. The discontinuity in the data near

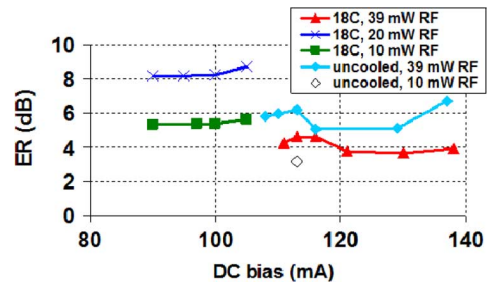


Fig. 7. Extinction ratio versus dc bias for 2.5-Gb/s modulation under different operating conditions.

105 mA occurs due to a mode hop (Fig. 4). The modulation characteristics change significantly on either side of the hop, indicated by the need for a higher RF power to maintain the same ER. We believe this change is related to the detuning from the reflectivity peak [8], which changes signs before and after mode hops.

#### IV. CONCLUSION

We demonstrated a DBF laser on the hybrid silicon evanescent platform operating at 1596 nm with a sidemode suppression ratio of 50 dB. The laser operates continuous wave with a lasing threshold of 65 mA and maximum output power of 11 mW at 15 °C. The laser generated open eye diagrams with extinction ratios of 8.7 and 5.5 dB for data rates of 2.5 and 4 Gb/s, respectively. These output characteristics are comparable to commercially available lasers. We believe this device is an attractive option for a directly modulated laser to be integrated with silicon electronics and arrayed waveguide gratings in order to create low cost, scalable, silicon wavelength division-multiplexed transmitters.

#### ACKNOWLEDGMENT

The authors would like to thank J. Shah, M. Haney, M. Paniccia, H. Park, and H.-W. Chen for insightful discussions.

#### REFERENCES

- [1] D. Pasquariello and K. Hjort, "Plasma-assisted InP-to-Si low temperature wafer bonding," *IEEE J. Sel. Topics Quantum Electron.*, vol. 8, no. 1, pp. 118–131, Jan. 2002.
- [2] Q. Tong, Q. Ga, G. Hudson, G. Fountain, and P. Enquist, "Low temperature InP/Si wafer bonding," *Appl. Phys. Lett.*, vol. 84, p. 732, 2004.
- [3] J. Van Campenhout *et al.*, "Electrically pumped InP-based microdisk lasers integrated with a nanophotonic silicon-on insulator waveguide circuit," *Opt. Express*, vol. 15, no. 11, pp. 6744–6749.
- [4] G. Roelkens, D. Van Thourhout, R. Baets, R. Nötzel, and M. Smit, "Laser emission and photodetection in an InP/InGaAsP layer integrated on and coupled to a silicon-on-insulator waveguide circuit," *Opt. Express*, vol. 14, pp. 8154–8159, 2006.
- [5] H. Park *et al.*, "Photonic integration on hybrid silicon evanescent device platform," *Advances Opt. Technol.*, p. 682978, 2008.
- [6] A. W. Fang, E. Lively, Y.-H. Kuo, D. Liang, and J. E. Bowers, "A distributed feedback silicon evanescent laser," *Opt. Express*, vol. 16, pp. 4413–4419, 2008.
- [7] M. Bass, *Handbook of Optics IV*. New York: McGraw-Hill, 2001, p. 9.4.
- [8] U. Feiste, "Optimization of modulation bandwidth in DBR lasers with detuned Bragg reflectors," *IEEE J. Quantum Electron.*, vol. 34, no. 12, pp. 2371–2379, Dec. 1998.